Journal of Metals, Materials and Minerals, 36(3), e2615, 2026

The effect of granule composition on the densification and strength of two different compacted 92% aluminas

Ryan MCCUISTON[1], and Kritkaew SOMTON[2,*]

[1] *King Mongkut's University of Technology Thonburi (KMUTT), Bangkok, 10140, Thailand*
[2] *National Metal and Materials Technology Center (MTEC), National Science and Technology Development Agency (NSTDA), Pathumthani, 12120, Thailand*

***Corresponding author e-mail**: kritkaes@mtec.or.th

Received date:
25 December 2025
Revised date:
22 February 2026
Accepted date:
25 March 2026

Keywords:
Alumina;
Granules;
Sintering;
Shrinkage;
Weight loss

Abstract

High-alumina (Al_2O_3) ceramics are an important, but sometimes overlooked industrial material. Two 92% alumina spray-dried granules, which contained different sintering aid compositions, were studied. The two alumina granules, called MT and JP, were die compacted to form bend bars and heated at temperatures from 200°C to 1600°C. The effect of the sintering aid composition on the shrinkage, density, and fracture strength of samples were investigated. It was found that MT samples had a lower density than the JP samples up to 1100°C, due to a greater weight loss following binder removal. However, between 1200°C to 1600°C, the MT samples had higher density (95.45%. vs. 94.40%), shrinkage (18.1% vs. 14.4%), and fracture strength (315 MPa vs. 264 MPa) than the JP samples, due to a 100°C lower onset of liquid phase sintering. An analysis using glass formation principles determined that the MT sintering aid contained more glass network modifiers and property modifiers, which likely reduced the sintering liquid formation temperature and viscosity.

1. Introduction

The manufacturing of advanced engineering ceramics by die pressing of spray-dried granules is widely used in industry [1,2]. For the case of spray-dried alumina (Al_2O_3), it is known that many factors, including the compaction pressure and granule strength [3], internal and external friction [4,5], as well as the part geometry and sintering temperature [6] can influence the shrinkage and densification of the compacted green body. From the work of Somton *et al.* [7], it was found that an increase of compaction pressure resulted in a decreased sintering shrinkage for a 92% alumina. While an increase of the organic binder content in the spray-dried granules increased the sintering shrinkage, due to increased porosity from the binder removal. The role of sintering aids on the shrinkage and densification behavior of the 92% alumina was not examined in that work. However, a more complete assessment of the shrinkage and densification characteristics of a ceramic is often necessary to better control the final dimensions of sintered parts.

The use of sintering aids in alumina is essential for achieving the desired microstructural features, such as grain size and distribution, grain boundary characteristics and porosity content. Many different sintering aids have been researched for alumina, such as CaO, SiO_2, MgO, Y_2O_3, La_2O_3, etc. [8]. Ding *et al.* [9] used kaolinite and calcium carbonate as sources of SiO_2 and CaO for sintering of a 95% alumina. An increase of volume shrinkage up to 39% and a compressive strength of 1323 MPa were found. Liu *et al.* [10] found that an increase of TiO_2 from 0% to 1% increased the linear sintering shrinkage of a 95% alumina from 4.83% to 16.65% and also increased the flexural strength. High-purity (~99% Al_2O_3) engineering aluminas often utilize a very small amount of a single oxide that functions as a solid state sintering aid. This is in contrast to the so called high-aluminas (~85% to 95% Al_2O_3) that typically use a larger amount of industrial minerals, that provide multiple oxides which function together to effectively liquid phase sinter the alumina [11].

While the high-purity engineering aluminas have many exceptional properties, they are typically more expensive to manufacture, due to stringent purity and processing requirements. The high-aluminas though, can offer acceptable properties at a lower cost, due to less stringent manufacturing requirements. These high-aluminas have been used in industrial wear and electrical applications [11,12]. This research, guided by glass formation principles, studied the effect of sintering aid composition of two spray-dried 92% high-alumina granules on the shrinkage, densification and fracture strength, as a function of sintering temperature.

2. Experimental

The sources of the 92% alumina granules used in this study were an in-house (MTEC) production granule called as MT here, and a commercially available granule supplied by Y.S. Company (Japan), called as JP here. The MT granules are intended as a lower cost, domestic alternative to the imported JP granules, while having comparable properties. The average sizes of the MT and JP granules were 66 µm and 54 µm in D [4,3], respectively, as measured by laser diffraction

particle size analysis (Malvern Mastersizer). The MT granules contains 8 wt% PVA binder system (Ghosenol, GL-05, Japan) and 8 wt% of mineral sintering additives, while the JP granules contains 5 wt% PVA binder system and 8 wt% of mineral sintering additives. Details on the MT granule preparation has been detailed previously [13]. The greater PVA binder content of the MT granules is for improved green body strength of compacted parts. The MT and JP granules contain alumina powders with an average particle size of less than 1 μm. The chemical compositions of the granules were characterized using X-ray fluorescence (XRF) and the results reported as the stoichiometric oxides.

The granules were uniaxially die pressed with a constant pressure of 133 MPa to produce rectangular, bend bar specimens with dimensions of 4 mm × 6 mm × 34 mm. Five specimens were produced for each condition tested. The samples were heated in air in a box furnace, at temperatures from 200°C to 1600°C, using a heating rate of 100°C·h^{-1}, with a hold time of 2 h. The test temperature range was divided from 200°C to 1000°C and from 1100°C to 1600°C and are referred to here as the pre-sintering and sintering temperatures, respectively.

The pre-sintered and sintered samples were measured for weight loss and dimensional shrinkage. The bulk density was calculated using the measured weight and dimensions of the samples. The bulk density and porosity were also measured using Archimedes' method for the samples sintered at 1000°C and above according to ASTM C373 [14]. The flexural strengths of the samples were measured in three-point bending with a universal testing machine (UTM: Instron 8872) with a span of 20 mm and loading rate of 0.05 mm·min^{-1}. The microstructures of the fracture surfaces of the samples were observed by scanning electron microscopy (SEM: Hitachi S-3400) at a magnification of 1000x. The phase content of sintered samples was characterized using X-ray diffraction (XRD) from 10 to 90°.

3. Results and discussion

3.1 Granule chemistry

The chemical compositions of the MT and JP granules, as determined by XRF, are shown in Table 1. The results are reported as the assumed stoichiometric oxide of the detected metal element. Both the MT and JP columns summed to 100.0%, which showed the oxide assumption to be valid. It was found that the Al_2O_3 content in the MT and JP granules were very close to the stated 92% purity level, at 92.4% and 92.1%, respectively. There were slight differences between the MT and JP granules for several oxides, such as Na_2O, Fe_2O_3, and MgO. However, there were two larger differences between the SiO_2 and CaO content in the MT and JP granules. The MT granules had SiO_2 and CaO contents of 3.8% and 2.6%, respectively, while the JP granules had a majority of SiO_2 at 6.1% and a small amount of CaO at 0.6%.

The XRF results were generally consistent with the previously reported [7] mineral additives used in these granules. For the MT granules, they were wollastonite ($CaSiO_3$), celsian ($BaO·Al_2O_3·2SiO_2$), and clay ($Al_2O_3·2SiO_2·2H_2O$), while for the JP granules, they were calcium carbonate ($CaO·CO_2$), talc ($3MgO·4SiO_2·H_2O$) and clay ($Al_2O_3·2SiO_2·2H_2O$). In the MT granules, the MgO, Na_2O and Fe_2O_3 were incidental additions, while Na_2O and Fe_2O_3 were likewise incidental additions in the JP granules. Their exact origin was not investigated, but they are common accessory mineral and/or ion impurities found in industrial minerals, such as clay [15,16].

For the sintering of Al_2O_3 containing a minor SiO_2 phase, the SiO_2 is expected to create a glassy liquid phase, which results in the liquid phase sintering of the Al_2O_3 [17]. The silica (SiO_2) phase can be augmented and modified in high-alumina ceramics with the addition of materials such as clay, wollastonite and talc, to create calcium and magnesium aluminosilicate liquids, which produce stronger and more refractory high-aluminas [11]. The barium in the celsian of the MT granule functions as a flux similar to calcium and magnesium, as it is also an alkaline earth element, but it can offer a different set of thermal and mechanical properties to the glassy phase [18]. In MT granules, the celsian is used for thermal expansion matching. The exact minerals used, besides for reasons of chemistry and properties, may also be selected for beneficial contributions to the compaction behavior, such as with talc and clay [11,16]. These mineral additions to the SiO_2, can be thought of as contributing oxides to the initial SiO_2 liquid phase much in the same way that they would to an ordinary silicate glass. It would therefore be beneficial to estimate the composition of the starting glassy liquid phase created from the sintering aids, to provide some insight into the liquid phase sintering process.

From the chemical compositions of the MT and JP granules, shown in Table 1, the minor oxides were used to calculate the starting liquid phase, i.e. glass composition, as shown in Table 2. The Al_2O_3 and 'Other' content were ignored in the calculation. The calculated compositions for the MT and JP liquid phases showed a number of key differences between them. In ordinary silicate glasses, the various oxides can be divided into different categories based on their role in the glass structure [19,20]. SiO_2 is a glass or network former and increasing its content increases the glass melt viscosity. Na_2O is a network modifier and it creates weak, non-bridging sodium–oxygen bonds, which reduce the viscosity and acts as a flux during melting. CaO is an intermediary or property modifier, and while it also creates non-bridging calcium–oxygen bonds, they are moderately strong and decrease viscosity when replacing SiO_2 or increase viscosity when replacing Na_2O. In greater amounts, some property modifiers can also act as weak fluxes. The MgO and BaO function similarly to CaO in a glass. Fe_2O_3 can act as either a network former or modifier depending on the content [21], and in this small amount is likely acting as a network modifier, similar to the Na_2O.

It can be seen in Table 2, that the calculated glass composition from the MT sintering aids is approximately 50% network former and 50% network modifier and property modifier, while for the JP sintering aids it is approximately 78% network former and 22% network modifier and property modifier. Based on these compositions, the MT sintering aids could be expected to produce a liquid phase at a lower temperature, due to the greater Na_2O and Fe_2O_3 content and to produce a lower viscosity liquid phase due to the greater combined network modifier and property modifier content. The JP sintering aids could be expected to form a liquid phase at a higher temperature and produce a higher viscosity liquid phase due to the smaller combined amount of network and property modifiers. This is with the assumption that the liquid phases are physically and chemically homogenous, as well as chemically stable. It is also with the understanding that the primary alumina particle sizes are comparable between MT and JP granules, as the liquid phase sintering rate can be affected by the particle size, in addition to the liquid phase chemistry.

Table 1. Chemical compositions of the MT and JP granules as determined by XRF.

Oxide	MT granule [wt%]	JP granule [wt%]
Al_2O_3	92.4	92.1
SiO_2	3.8	6.1
CaO	2.6	0.6
MgO	0.4	0.9
Na_2O	0.4	0.1
Fe_2O_3	0.1	0.1
BaO	0.2	0.0
Other	0.1	0.1
Sum	100.0	100.0

Table 2. Calculated glass composition of the liquid phase for the MT and JP granules.

Oxide	MT glass [wt%]	JP glass [wt%]
SiO_2	50.67	78.21
CaO	34.67	7.69
MgO	5.33	11.54
Na_2O	5.33	1.28
Fe_2O_3	1.33	1.28
BaO	2.67	0.00
Sum	100.00	100.00

3.2 Sintered sample phase content

The XRD results for MT and JP samples sintered at 1600°C, are shown in Figure 1. For the MT sample, Figure 1 (top), the pattern was matched with corundum (α-Al_2O_3) (ICDD PDF# 00-042-1468) and a minor amount of wollastonite ($CaSiO_3$) (ICDD PDF# 00-027-0088). The wollastonite phase was likely from undissolved wollastonite added to MT granules. For the JP sample, Figure 1 (bottom) the pattern was matched with corundum (α -Al_2O_3) (ICDD PDF# 00-042-1468) and minor amounts of quartz (α-SiO_2) (ICDD PDF# 01-077-1062) and cordierite ($Mg_2Al_4Si_5O_{18}$) (ICDD PDF# 00-060-0061). The quartz was likely from undissolved particles contained as an accessory phase in the mineral sintering additives, such as the clay [15,16]. The very minor amount of cordierite was likely formed from the liquid phase.

The XRD patterns in Figure 1 showed that the sintering additives in the MT sample, celsian and clay, were completely dissolved, while the wollastonite was nearly completely dissolved during sintering. For the JP sample, the sintering additives, calcium carbonate, talc and clay, were completely dissolved during sintering. The small amount of solidified liquid phase in the MT and JP samples, approximately 10 vol% to 12 vol%, would not be expected to generate a large amorphous hump in the XRD patterns, but could be responsible for the slightly elevated background signal seen at low theta angles from ~10° to 30° [22]. The XRD patterns also showed that the solidified liquid phase remained nearly completely amorphous during solidification, with only the previously mentioned minor amount of wollastonite in the MT sample and the minor amounts of quartz and cordierite in the JP sample. The XRD results supported a glass analysis approach to the sintering liquid.

3.3 Densification behavior

Plots of the average weight loss and linear shrinkage as a function of temperature, for the MT and JP samples, are shown in Figure 2. The weight loss had standard deviations of approximately ±0.05% and ±0.11% for MT and JP samples, respectively, while the shrinkage had standard deviations of approximately ±0.08% and ±0.04% for MT and JP samples, respectively. The small values of the standard deviation result in bars that are generally obscured by the point markers in Figure 2. The small standard deviations indicated good sample and measurement reproducibility. It was found that the MT samples had a greater weight loss and shrinkage than the JP samples for the entire temperature range of 200°C to 1600°C. The MT samples from 200°C to 1000°C had a maximum shrinkage of 0.7% which was slightly greater than the 0.3% maximum shrinkage of the JP samples in the same temperature range. The weight loss, due primarily to binder removal from the granules, did not strongly affect the shrinkage in the pre-sintering temperature range up to 1000°C. During sintering, beyond 1000°C, the MT samples shrank rapidly from 1.7% at 1100°C to 16.5% at 1400°C and reached a maximum shrinkage of 18.1% at 1600°C. The JP samples shrank from 0.6% at 1100°C to 4.0% at 1300°C. After that, the JP samples shrank rapidly to 13.7% at 1500°C and reached a maximum shrinkage of 14.4% at 1600°C.

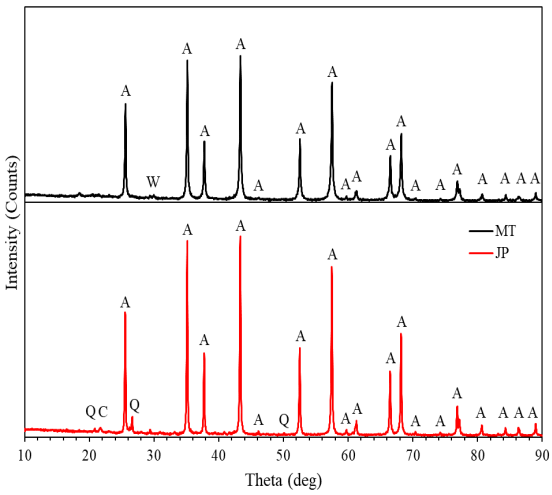

Figure 1. XRD patterns of MT (top) and JP (bottom) samples sintered at 1600°C. The peaks are identified as A = alumina, C = cordierite, Q = quartz and W = wollastonite.

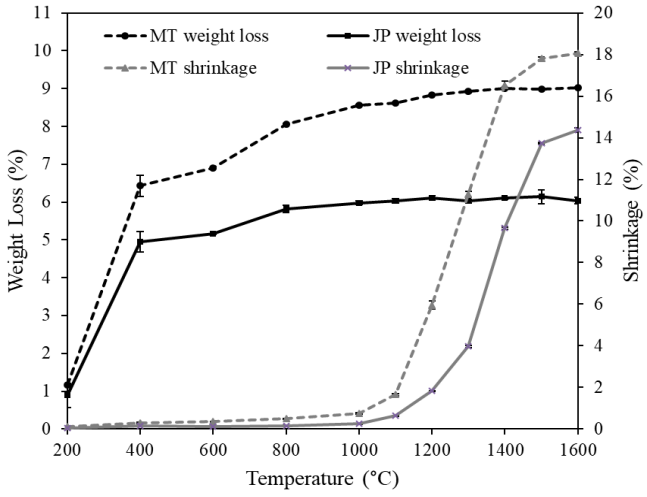

Figure 2. Plots of weight loss and linear shrinkage vs. temperature for the MT and JP samples.

The weight loss due to binder removal, as well as sintering aid decomposition processes, resulted in the creation of porosity in the samples. At pre-sintering temperatures, there was little thermal energy to contribute to the shrinkage process, such that the porosity was reduced very little. However, at the higher sintering temperatures, the creation of a liquid phase would be expected to rapidly fill the porosity and contribute to shrinkage. A point for point comparison of the MT and JP samples in the sintering temperature range showed that the MT samples experienced a more rapid shrinkage onset at 1100°C and a greater total amount of shrinkage. This indicated the creation of a liquid phase with a lower viscosity and/or in a greater volume in the MT samples than in the JP samples. This result concurred with the previous assessment based on the calculated glass compositions.

Plots of the average bulk density of the MT and JP samples, as a function of temperature, are shown in Figure 3. The standard deviations of the calculated and Archimedes bulk densities were very small, approximately ±0.01 g·cm^{-3}, and are not readily visible in Figure 3, due to point marker obscuration. The starting green density of the MT sample was 2.28 g·cm^{-3}, which was lower than the 2.42 g·cm^{-3} green density of the JP sample. This was mostly due to a greater content of PVA binder (ρ = 1.2 g·cm^{-3}) in the MT sample than the JP sample, as confirmed by the weight loss in Figure 2. There was a reduction in density for both MT and JP samples that began in the temperature range of 200°C to 400°C, due to the large weight loss combined with only a minimal amount of sample shrinkage, i.e. decreased volume. The MT samples had a 5.3% density reduction which was slightly greater than the 4.2% density reduction of the JP samples, due to the slightly greater weight loss of the MT over the JP samples. The MT and JP sample densities remained stable until 1000°C, as both their weight loss and volumes were largely unchanged. The MT sample density increased from 2.20 g·cm^{-3} at 1100°C to 2.54 g·cm^{-3} at 1200°C before it rapidly increased to 3.55 g·cm^{-3} at 1400°C and reached a maximum density of 3.72 g·cm^{-3} at 1600°C. The JP sample density increased slightly from 2.33 g·cm^{-3} at 1100°C to 2.42 g·cm^{-3} at 1200°C and then increased moderately to 3.08 g·cm^{-3} at 1400°C and reached a maximum density of 3.62 g·cm^{-3} at 1600°C. In the sintering temperature region, the rapid liquid phase formation in the MT samples allowed for quicker densification compared with the JP samples, with comparable densities of MT and JP samples being shifted by approximately 100°C. Again, this result agreed with the previous glass composition assessment.

The density plots in Figure 3 for the MT and JP samples were well correlated with the measured shrinkage curves seen in Figure 2, especially in the sintering temperature region between 1100°C and 1600°C. The final density of 3.72 g·cm^{-3} for the MT sample at 1600°C was greater than the final JP sample density of 3.62 g·cm^{-3}, due in part to the greater shrinkage of MT compared with JP.

Lastly, the average bulk densities of the MT and JP samples were also determined using Archimedes method, as shown in Figure 3. The Archimedes method was not used for samples in the pre-sintering temperature region due to their mechanical weakness in the binder removed state before significant sintering had occurred. The bulk density, as measured by Archimedes, agreed well with the bulk density that was calculated from the mass and dimensional measurements of the MT and JP samples. The Archimedes measurements confirmed the validity of the bulk density calculations.

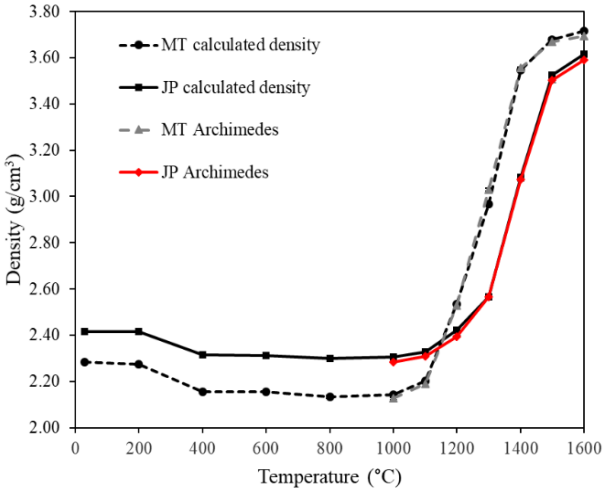

Figure 3. Plots of bulk density vs. temperature for the MT and JP samples.

Using an additivity relationship method of Huggins and Sun [23], the densities were calculated for the MT and JP glass compositions shown in Table 2. It was assumed that all of the oxide phases, with the exception of Al_2O_3, were incorporated into the glasses. From the glass compositions, the densities were calculated to be 2. g·cm^{-3} and 2.458 g·cm^{-3} for MT and JP glasses, respectively. The density of fused silica (100% SiO_2) glass is 2.20 g·cm^{-3} and the addition of both network and property modifiers, such as Na_2O and CaO, increases the density [19,20]. The density of the MT glass was greater than the JP glass due primarily to the large CaO content.

With the calculated theoretical densities of the MT and JP glasses, and an Al_2O_3 theoretical density of 3.99 g·cm^{-3}, the theoretical densities (ρ_{th}) of the MT and JP samples were calculated according to Equation (1) as,

$$\rho_{th} = V_G\rho_G + V_A\rho_A \quad (1)$$

where V_G and V_A are the volume fractions and ρ_G and ρ_A are the theoretical densities of the glasses (G) and alumina (A), respectively. These calculations assumed that the glassy phase remained amorphous and did not crystallize. Based on the XRD results shown in Figure 1, this was a reasonable assumption. The MT sample contained 89.7 vol% Al_2O_3 and 10.3 vol% glass. The estimated theoretical density of the MT sample was calculated to be 3.871 g·cm^{-3}. The JP sample contained 87.9 vol% Al_2O_3 and 12.1 vol% glass. The estimated theoretical density of the JP sample was calculated to be 3.805 g·cm^{-3}. While the theoretical densities of the MT and JP glasses are different, the theoretical densities of the MT and JP samples are more similar due to the large amount of alumina. The MT sample had a slightly greater calculated theoretical density, but the theoretical density of JP sample was still within 2% of it.

Using the calculated theoretical densities of the MT and JP samples, the percent of theoretical density (%ρ_{th}) was calculated at 1100°C, 1200°C, 1400°C and 1600°C, as shown in Table 3. The %ρ_{th} was calculated according to Equation (2) as,

$$\%\rho_{th} = \frac{\rho_b}{\rho_{th}} \times 100 \quad (2)$$

Table 3. Various calculated density values for the sintered MT and JP samples.

Calculated value		MT	JP
Glass phase density [g·cm^{-3}]		2.831	2.458
Sample theoretical density [g·cm^{-3}]		3.871	3.805
%Theoretical Density [%]	1600°C	95.45	94.40
	1400°C	91.85	80.80
	1200°C	65.27	62.93
	1100°C	56.59	60.71

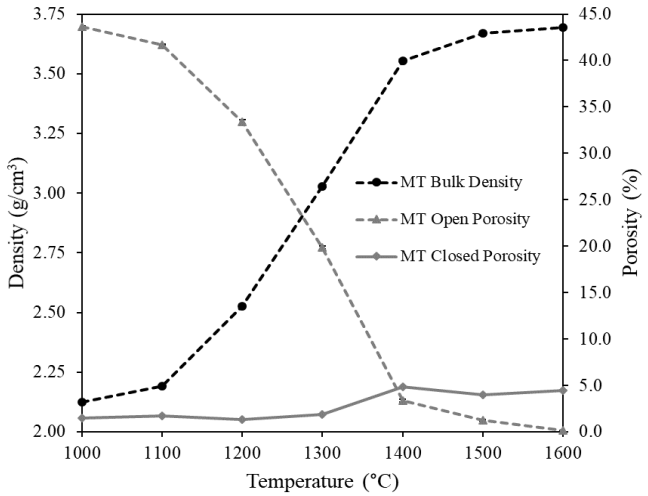

Figure 4. Plots of open and closed porosity, as well as bulk density, for MT samples as a function of temperature.

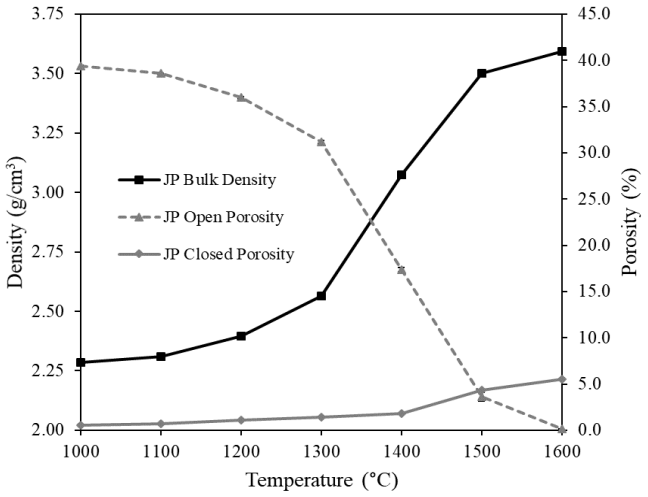

Figure 5. Plots of open and closed porosity, as well as bulk density, for JP samples as a function of temperature.

where ρ_b and ρ_{th} are the bulk and theoretical densities, respectively. At 1100°C, the $\%\rho_{th}$ of MT was 56.59%, and JP had a slightly higher $\%\rho_{th}$ of 60.71%. At 1200°C, the $\%\rho_{th}$ values crossed and MT had a $\%\rho_{th}$ of 65.27%, which was slightly greater than the $\%\rho_{th}$ of 62.93% for JP. At 1400°C, the $\%\rho_{th}$ of MT rapidly increased to 91.85% while for JP it was a more moderate 80.80%. The increase of the $\%\rho_{th}$ values of the MT and JP samples matched their respective density trend lines as seen in Figure 3. This was due to the similarity of the theoretical densities of MT and JP samples. At 1600°C the maximum $\%\rho_{th}$ was 95.45% for the MT sample and 94.40% for the JP sample. The MT sample achieved a slightly greater sintered density than the JP sample, on a percentage basis. The calculated theoretical densities of MT and JP samples were both in reasonable agreement with reported densities of various high-aluminas in the 92% purity range [11,24,25].

Archimedes method [14] was used to determine the bulk (ρ_b) and apparent density (ρ_a), as well as the percent open porosity ($\%P_O$) of the MT and JP samples. Using that data, the percent closed porosity ($\%P_C$) content was calculated according to Equation (3) as,

$$\%P_C = \rho_b \left[\frac{1}{\rho_a} - \frac{1}{\rho_{th}}\right] \times 100 \quad (3)$$

where ρ_b, ρ_a, and ρ_{th} are the bulk, apparent and theoretical densities, respectively.

Plots of the average bulk density, as well as the open and closed porosities of the MT and JP samples from 1000°C to 1600°C, are shown in Figure 4-5, respectively. As the standard deviations of the density measurements were small, calculations using the density also had small standard deviations, approximately ±0.2% to ±0.5%, and are not readily visible in Figures 4-5 due to point marker obscuration. The MT and JP samples both displayed the same general trends. The bulk density and open porosity were inverses of each other. When the bulk density was low, it was due to a greater amount of open porosity, as would be expected for compacted powder green bodies. Both MT and JP samples had a larger amount of open rather than closed porosity at the sintering temperatures from 1000°C to approximately 1400°C for the MT samples and from 1000°C to approximately 1500°C for the JP samples. The temperatures of 1400°C and 1500°C for MT and JP samples respectively, were the transition from more open to more closed porosity. The few percent of porosity that remained in both the MT and JP samples was closed porosity. The measurable open porosity was completely eliminated, which indicated a high degree of vitrification of the samples.

The slope changes at the transition temperatures of the bulk density curves of the MT and JP samples, seen Figure 4-5, indicated that the densification rate slowed down. This was potentially due to the negative contribution to sintering by air-filled closed pores, a result of the sintering atmosphere [26]. It was observed by Coble [27] that solid state sintered alumina failed to reach full density when sintered it air. It was attributed to the lack of nitrogen solubility (Air is ~78% N_2) in the alumina. More recently it was also shown that alumina sintered with 10 vol% and 20 vol% of a calcium aluminosilicate glass also failed to reach full density when sintered in air [28]. This was attributed to pressurization of the air trapped in the closed porosity, again a side effect of poor nitrogen solubility in both the alumina and the glass phases. In both cases, full density could be achieved by sintering in vacuum or with an atmosphere containing a soluble gas, such as hydrogen.

3.4 Flexural strength

Figure 6 shows plots of the average flexural strengths of the MT and JP samples as a function of temperature. Both the MT and JP samples had low strengths of approximately 1 MPa to 7 MPa in the pre-sintering temperature range. This would be expected as only a small amount of particle necking would take place at these relatively

low temperatures. When the temperature was increased above 1000°C though, the MT samples had a rapid increase of strength from 12 MPa at 1100°C to 308 MPa at 1500°C and then a slight increase of strength to 315 MPa at 1600°C. The JP samples had an increase of strength from 8 MPa at 1100°C to 32 MPa at 1300°C, followed by a rapid increase of strength to 264 MPa at 1600°C. The flexural strength values of the MT and JP samples at 1600°C are in line with the reported values for various 92% purity aluminas [11,24,25]. The standard deviations of the strength measurements were reasonably small, approximately ±8% and ±12% of the average strength values at each temperature, for MT and JP samples, respectively.

The flexural strength increases in the sintering temperature range were a direct result of the density increases, i.e. porosity reduction due to sintering, in the MT and JP samples. It is well known that the presence of microstructural porosity in ceramics decreases flexural strength. As the MT samples were denser, as a percentage of the theoretical density, than the JP samples at a given temperature, the MT sample strengths were therefore also greater. There can be other factors influencing the flexural strength though, such as grain size, but they were not explored here. It is also pointed out that the MT strength curve appeared to begin plateauing at 1600°C and a further increase in sintering temperature may not yield further significant gains in strength. However, the JP strength curve appeared to still be increasing and may benefit from an increased sintering temperature. This can be understood when the JP glass composition, shown in Table 2, is considered. The decreased amount of network and property modifiers would make the JP liquid phase more refractory and it would therefore have a greater liquid phase viscosity at the same temperature when compared with the MT glass composition. This increased viscosity would hinder particle rearrangement and densification.

3.5 Sintered microstructure

SEM images of the fracture surfaces of the MT and JP flexural strength samples sintered from 1000°C to 1600°C are shown in Figure 7. At 1000°C, both the MT and JP samples clearly showed the exterior surfaces of the deformed spray-dried granule relics, with little indication of neighboring granules having been bonded together due to sintering. At 1200°C, the MT sample showed some areas of fracture at the granule relic contact points, which indicated an amount of granule necking had occurred. The JP fracture surface had no visible indication of granule necking. For both MT and JP samples, at sintering temperatures of 1000°C and 1200°C, the fracture surfaces appeared predominantly inter-granule in nature, i.e. the fracture path was between the exterior surfaces of the spray-dried granule relics. At 1400°C and 1600°C though, the fracture surfaces were largely intra-granule in nature, i.e. the fracture path cut through the granule relics, rather than in between them as previously observed at 1000°C and 1200°C.

In the MT and JP samples sintered at 1000°C and 1200°C there was also seen a large amount of open, inter-granule porosity as well, i.e. pores between the granule relics. At 1400°C, the amount of inter-granule porosity was greatly reduced in the MT sample, while the JP sample still displayed large pores between the granules. In the JP sample at 1400°C, a large amount of intra-granule porosity was also seen, i.e. pores within the granule relics. At 1600°C, both MT and JP samples appeared fairly well sintered, with the visible porosity being closed, inter-granule porosity. These larger, inter-granule pores are characteristic of spray-dried granule compacts and could be removed in several ways, including increased sintering temperature and/or time, or with an increased compaction pressure.

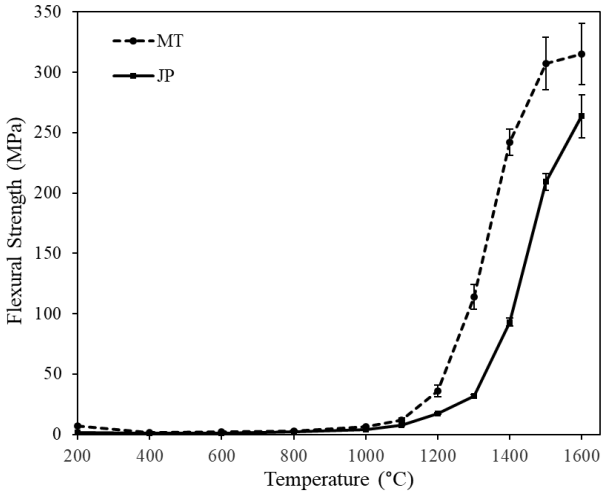

Figure 6. Plots of flexural strength vs. temperature for the MT and JP samples.

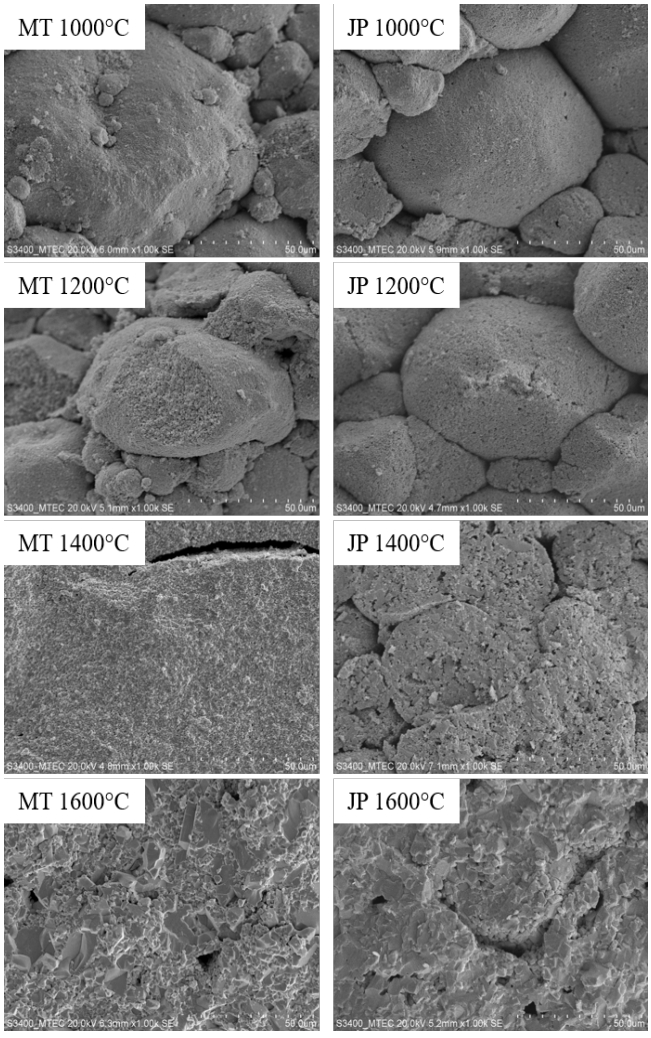

Figure 7. SEM images of the fracture surfaces of MT and JP samples sintered at 1000°C, 1200°C, 1400°C, and 1600°C.

The microstructures observed in Figure 7 were consistent with the shrinkage, density and fracture strength results. The MT samples sintered to a lower porosity than the JP samples, which resulted in increased shrinkage, density and fracture strength. The chemistry of the liquid sintering phase, when viewed as a glass, also supported these results. The increased network and property modifier content within the mineral sintering aids of the MT samples created an appreciable liquid phase at a temperature approximately 100°C lower than the JP samples. This is seen in the SEM images as less porosity in the MT samples than the JP samples for the same temperature.

4. Conclusions

The influence of the sintering aid chemical composition on the shrinkage, densification, and flexural strength of die pressed 92% alumina, from two different granule sources, has been studied. The conclusions were as follows:

The greater binder content of the MT granules resulted in lower green and pre-sintered densities, as well as higher weight loss, than the JP granules. This occurred from room temperature to 1100°C.

The porosity created by the binder removal was not reduced at pre-sintering temperatures below 1000°C. The porosity was reduced, i.e. the shrinkage increased, in the sintering temperature range due to the onset of liquid phase sintering.

The greater shrinkage of MT samples in the sintering range was due to the sintering aid selection. When viewed as a glass composition, the MT samples had a greater network and property modifier content, which created a sintering liquid at a 100°C lower temperature. The JP samples had a more refractory glass composition, due to the sintering aid selection.

The greater shrinkage of the MT samples resulted in higher density and strength than the JP samples, for the same sintering temperature. Observing the fracture surfaces confirmed that the MT samples had improved particle necking at pre-sintering temperatures and reduced porosity at sintering temperatures compared to the JP samples.

The application of glass formation principles and glass theoretical density calculations, when combined with simple porosity calculations, can be a useful tool for the analysis of liquid phase sintered alumina ceramics. This is with the understanding that not all assumptions made may be valid.

Acknowledgements

The authors would like to thank the National Metal and Material Technology Center (MTEC) a member of National Science Technology Development Agency (NSTDA), Thailand, for providing funding for this research and for access to testing facilities.

References

[1] R. Oberacker. "*Powder compaction by dry pressing,*" in Ceramic Science and Technology: Synthesis and Processing, vol. 3, Wiley-VCH, Germany, pp. 3–37, 2012.

[2] M. Dondi, "*Powder granulation and compaction*," in Encyclopedia of Materials: Technical Ceramics and Glasses, vol. 1, Elsevier Inc., pp. 136–145, 2021.

[3] D. E. Niesz, "A review of ceramic powder compaction," *KONA Powder and Particle Journal*, vol. 14, pp. 44–51, 1996.

[4] S. Balasubramanian, D. J. Shanefield, and D. E. Niesz, "Effect of internal lubricants on defects in compacts made from spray-dried powders," *Journal of the American Ceramic Society*, vol. 86, no. 1, pp. 134–138, 2002.

[5] S. Balasubramanian, D. J. Shanefield, and D. E. Niesz, "Effect of externally applied plasticizer on compaction behavior of spray-dried powders," *Journal of the American Ceramic Society,* vol 86, no. 4, pp. 749–754, 2002.

[6] K. Somton, K, Dateraksa, and R. McCuiston, "A study of alumina spray dried granules on packing density and sintering shrinkage of simple and complex shape," *Key Engineering Materials*, vol. 608, pp. 175–180, 2014.

[7] K. Somton, K. Dateraksa, P. Laoratanakul, and R. McCuiston, "Shrinkage and properties of die pressed alumina produced from different granule sources," *AIP Conference Proceedings*, vol. 2279, pp. 1–7, 2020.

[8] C. Qian, K. Hu, Z. Shen, Q. Wang, P. Li, and Z. Lu, "Effect of sintering aids on mechanical properties and microstructure of alumina ceramic via stereolithography," *Ceramics International*, vol. 49, no.11, pp. 17506–17523, 2023.

[9] D. Ding, Y. Guan, G. Xiao, Z. Mao, X. Shi, K. Gao, X. Chong, J. Luo, and C. Lei, "Effects of sintering temperature on micro-structure and mechanical properties of pressureless sintering alumina ceramics with Al_2O_3–SiO_2–CaO sintering aids," *Refractories and Industrial Ceramics*, vol. 64, no. 2, pp. 136–146, 2023.

[10] N. Liu, X. Sun, Z. Chen, Z. Xu, N. Dai, G. Shi, S. Cai, X. Lv, and C. Zheng, "Direct ink writing of dense alumina ceramics prepared by rapid sintering," *Ceramics International*, vol. 48, no. 20, pp. 30767–30778, 2022.

[11] J. B. Wachtman, and R. A. Haber, "Advanced ceramics involving alumina," in Alumina Chemicals: Science and Technology Handbook, L.D. Hart Ed., The American Ceramic Society, Inc., pp. 329–335, 1990.

[12] E. Dörre, and H. Hübner, "*Alumina: Processing, Properties, and Application*s," Springer-Verlag, Germany, 1984.

[13] K. Somton, K. Dateraksa, D. Atong, and R. McCuiston, "The effect of granule morphology and composition on the compaction behavior and mechanical properties of 92% alumina spray dried granules," *Journal of Metals, Materials and Minerals*, vol. 22, no. 2, pp. 41–47, 2012.

[14] ASTM C373 Standard test method for water absorption, bulk density, apparent porosity, and apparent specific gravity of fired whiteware products, Annual Book of ASTM Standards, West Conshohocken, PA, USA, 2006.

[15] H. H. Murray, "*Clays*," in Ullmann's Encyclopedia of Industrial Chemistry, Wiley-VCH, Germany. pp. 1–34, 2012.

[16] J. S. Reed, "*Principles of ceramic processing*", 2nd ed., John Wiley & Sons, NY, USA, 1995.

[17] W. R. Cannon, E. Gugel, G. Leimer, G. Woetting, and R. Heimann, "*Ceramics, advanced structural products*," in Ullmann's Encyclopedia of Industrial Chemistry, Wiley-VCH, Germany, pp. 1–34, 2011.

[18] L. Barbieri, A. Bomartini Corradi, C. Leonelli, T. Manfredini, M. Romagnoli, and C. Siligardi, "The microstructure and mechanical properties of sintered celsian and strontium-celsian glass-ceramics," *Material Research Bulletin*, vol. 30, no. 1, pp. 27–41, 1995.

[19] J. E. Shelby, "*Introduction to glass science and technology*," 2nd ed., The Royal Society of Chemistry, UK., 2005.

[20] A. K. Varshneya, and J. C. Mauro, "*Fundamentals of Inorganic Glasses*," 3rd ed., Elsevier Inc., 2019.

[21] R. McCuiston, W. Nonthathi, and C. Auechalitanukul, "Forming and properties of glasses made from two Thai bottom ashes," *Suranaree Journal of Science and Technology*, vol. 31, no. 1, pp. 1–13, 2024.

[22] R. E. Dinnebier, and S. J. L. Billinge, "*Powder Diffraction, Theory and Practice*," The Royal Society of Chemistry, UK., 2008.

[23] M. L. Huggins, and K. H. Sun, "Calculation of density and optical constants of a glass from its composition in weight percentage," *Journal of the American Ceramic Society*, vol. 26, no. 1, pp. 4–11, 1943.

[24] R. Morrell, "*Handbook of Properties of Technical & Engineering Ceramics, Part 2. Data Reviews*, *Section I. High-Alumina ceramics*," H.M. Stationary Office, London, U.K., 1987.

[25] A. M. Abyzov, "Aluminum oxide and alumina ceramics (Review). Part 1. Properties of Al_2O_3 and commercial production of dispersed Al_2O_3," *Refractories and Industrial Ceramics*, vol. 60, no. 1, pp. 24–32, 2019.

[26] W. Dong, H. Jain, and M. P. Harmer, "Liquid phase sintering of alumina, I. microstructure evolution and densification," *Journal of the American Ceramic Society*, vol. 88, no. 7, pp. 1702–1707, 2005.

[27] R. L. Coble, "Sintering alumina: Effect of atmospheres," *Journal of the American Ceramic Society*, vol. 45, no. 3, pp. 123–127, 1962.

[28] W. Dong, H. Jain, and M. P. Harmer, "Liquid phase sintering of alumina, III. effect of trapped gases in pores on densification," *Journal of the American Ceramic Society*, vol. 88, no. 7, pp. 1714–1719, 2005.